


## Article

# Effect of Ultrasonic Vibration on Grain Size and Precipitated Phase Distribution of 6061 Aluminum Alloy Welded Joint

Chufan Sui <sup>1</sup>, Zhengjun Liu <sup>1,\*</sup> , Xingyu Ai <sup>1</sup>, Changjun Liu <sup>2</sup> and Zongxuan Zou <sup>1</sup>

<sup>1</sup> School of Materials Science and Engineering, Shenyang University of Technology, Shenyang 110870, China; suichufan@126.com (C.S.); 18809816959@163.com (X.A.); 15942492610@163.com (Z.Z.)

<sup>2</sup> Chemical Equipment Institute, Shenyang University of Technology, Liaoyang 111000, China; 18941998881@126.com

\* Correspondence: liuzhengjun1962@163.com

**Abstract:** To improve the weldability of 6061 aluminum alloy and improve the mechanical properties of welded joints, ultrasonic was introduced into the welding process. The microstructure changes of welded joints under different ultrasonic power were studied, and their effects on the mechanical properties of welded joints were analyzed. The grain size was calculated, and the distribution of precipitated phases was observed by the EBSD technique. The results show that the cavitation and acoustic flow produced by ultrasonic vibration can refine the microstructure of welded joint, reduce the grain size by nearly 50%. It promotes the transition of alloy elements to weld and eliminates the segregation of the strengthening phase to the grain boundary, thus improving the mechanical properties of the welded joint.

**Keywords:** ultrasonic vibration; aluminum alloy; welded joints; grain refinement; intensified phase



**Citation:** Sui, C.; Liu, Z.; Ai, X.; Liu, C.; Zou, Z. Effect of Ultrasonic Vibration on Grain Size and Precipitated Phase Distribution of 6061 Aluminum Alloy Welded Joint. *Crystals* **2022**, *12*, 240. <https://doi.org/10.3390/cryst12020240>

Academic Editors: Bolv Xiao and Enrique Maciá Barber

Received: 27 December 2021

Accepted: 8 February 2022

Published: 10 February 2022

**Publisher's Note:** MDPI stays neutral with regard to jurisdictional claims in published maps and institutional affiliations.



**Copyright:** © 2022 by the authors. Licensee MDPI, Basel, Switzerland. This article is an open access article distributed under the terms and conditions of the Creative Commons Attribution (CC BY) license (<https://creativecommons.org/licenses/by/4.0/>).

## 1. Introduction

Hard aluminum alloy is an ideal lightweight structural material due to its high strength, hardness, and low density. It is widely used in aerospace, automobile manufacturing, and rail transit. However, because of the excellent thermal conductivity of aluminum alloy, large heat input is required during welding. There is recrystallization in the fusion zone of the weld and over-aging softening in the heat-affected zone, and the strength coefficient of the welded joint is significantly reduced [1]. It was found that the center microstructure of the heat-treated aluminum alloy weld zone was mainly equiaxed grain, and the second phase was precipitated at the grain boundary. There was a segregation phenomenon of uneven chemical composition in the weld metal, the heat-affected zone of the joint was obvious softened, and the microstructure near the weld zone was recrystallized [2]. Thus, the joint strength usually does not exceed 60% of the base metal strength.

Schempp et al. [3] achieved grain refining by adding a commercial grain refiner containing titanium and boron to the GTA weld metal of aluminum alloy 6082. The weld metal mean grain size could be reduced significantly from about 70  $\mu\text{m}$  to a saturated size of 21  $\mu\text{m}$ . Aldalur et al. [4,5] through the gas metal arc welding (GMAW)-based WAAM technical process to improve the weldability of aluminum alloy, it showed its ability for the manufacture of parts by WAAM. However, WAAM technology also has problems such as process installation and residual stresses, which restrict the surface roughness and mechanical properties of parts. Lei et al. [6] used ultrasonic vibration-assisted laser welding technology to weld AZ31B magnesium alloy. Ultrasonic vibration increases the number of nucleation particles and refine grain, which improve the mechanical properties of welded joint.

Applying vibration to alloy melt is one of the effective methods to improve the internal structure and microstructure of metal materials. Ultrasonic wave is a kind of sound wave with frequency higher than 20 kHz. It has good directionality, strong penetrating ability,

and can easily obtain concentrated acoustic energy [7]. In the process of metal solidification, the effects produced by ultrasonic vibration mainly include cavitation effect, acoustic flow effect, mechanical effect, and thermal effect [8,9]. Acoustic cavitation is the main reason for increasing nucleation rate and refining microstructure. Acoustic flow effect and mechanical effect increase convection, reduce the temperature gradient in micro-area of melt, which is conducive to refining the grain, eliminating segregation and affecting grain growth. Most studies showed that ultrasound on the metal melt grain refinement mechanism is mainly the result of the cavitation effect and acoustic flow effect together [10–12]. Numerous studies at home and abroad put forward the following two theories on the basis of ultrasonic cavitation [13–16]:

- (1) **Crushing theory:** A large number of bubbles formed by high-energy ultrasound collapse and generate shock waves under the action of sound pressure exceeding a certain threshold, breaking the crystallized grown grains and making the grains get refined.
- (2) **Undercooling nucleation theory:** Some studies showed that the increase of cavitation bubbles generated by ultrasonic waves and evaporation of internal liquid will reduce the temperature of cavitation bubbles, which will lead to a decrease in the temperature of metal melt on the surface of cavitation bubbles. Therefore, it is possible to form crystal nucleus near the cavitation bubbles.

As they all involve the solidification process of metal and are all as-cast structure, welding can be regarded as “micro-casting”, and ultrasonic vibration can be introduced into the welding pool of aluminum alloy to improve welding defects. The current research mainly focuses on the influence of ultrasonic on friction stir welding, and the influence mechanism of ultrasonic vibration on fusion welding is still lacking. Combined with the characteristics of conventional TIG welding and ultrasonic vibration-assisted welding, the ultrasonic TIG composite welding method was proposed. In this work, an ultrasonic-assisted welding work platform was designed, which was used as a fixture and also as an ultrasonic vibration source, so as to introduce ultrasonic vibration into the welding pool. ER5356 welding wire was used to perform ultrasound-assisted TIG flat-butt experiments on 6061 aluminum alloy to investigate the effect of different ultrasonic powers on the mechanical properties and microstructure of the welded joints [17].

## 2. Materials and Methods

### 2.1. Materials and Welding Process

In the experiment, 6061-T6 (solution treatment + artificial aging) aluminum alloy was selected as the base material, the main component was Al-Mg-Si, the plate size was 125 mm × 125 mm × 5 mm, the mechanical properties were shown in the Table 1. ER5356 welding wire was used for welding, its Mg content was ~5%. The transition to metal weld in the form of droplets can increase the hardness of weld joints, which had a great effect on improving the softening of weld joints. The increase of Ti element content was also beneficial to grain refinement. The chemical compositions of base metal and welding wire were shown in the Table 2.

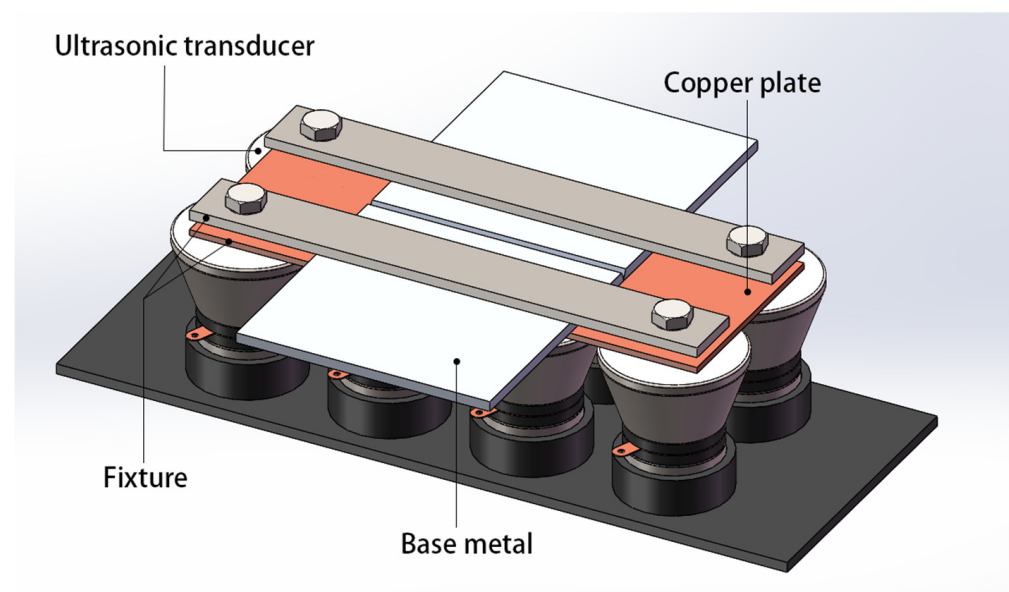
The welding machine used in the experiment was the WES-500 inverter argon arc welding machine. The welded joint was in the form of a butt joint, with a welding current of 110 A and argon flow rate of 12 L/min. In addition, an ultrasonic vibration auxiliary system was added as shown in Figure 1. Ultrasonic vibration was added to the inside of the molten pool during the welding process. The ultrasonic wave was directly introduced into the molten pool through the base metal, which overcomes the shortcomings of arc instability and low utilization rate of ultrasonic energy in the arc ultrasonic method, and can have a beneficial effect on the microstructure and mechanical properties of the weld to a greater extent.

**Table 1.** Mechanical property of 6061 alumina alloy.

	Tensile Strength/Mpa	Yield Strength/Mpa	Elongation/%	Hardness/HV
Standard value	310	275	12	95
Measured value	315	295	14	100

**Table 2.** Chemical composition of base metal and welding wire.

Material	Si	Fe	Cu	Mg	Mn	Zn	Ti	Cr	Al
6061	0.22	0.44	0.10	2.63	0.11	0.10	-	0.28	margin
ER5356	0.05	0.13	0.01	4.89	0.15	0.01	0.01	0.12	margin

**Figure 1.** Schematic diagram of ultrasonic vibration auxiliary system.

The ultrasonic output powers of 0 W, 160 W, 320 W, 480 W, 640 W, and 800 W were applied to the back of the base metal for welding. The ultrasonic source was eight ultrasonic transducers with the same power connected in parallel to increase the total ultrasonic output power and were synchronously adjusted by the KMD-K1 ultrasonic power supply. The model of the ultrasonic transducer is KMD-28100. The transducer was divided into two layers—upper and lower layers—and the middle was two ceramic vibrating plates. The piezoelectric effect of the ceramic plates converted the electrical energy into mechanical energy (i.e., ultrasonic wave), and then transmitted the ultrasonic wave through the upper cover. Under the high-frequency AC power supply, high-frequency mechanical vibration can be generated, and the vibration frequency was fixed at 28 kHz. Due to the low attenuation coefficient of ultrasonic waves in copper and the fast heat dissipation rate of copper, the softening effect of thermal cycling on the heat-affected zone was reduced. The ultrasonic vibration was transmitted into the molten pool through the copper pad, and it was used as a fixture to fix the base metal to prevent the deforming of aluminum alloy sheet.

## 2.2. Mechanical Properties Test

Hardness and tensile tests were mainly used to test the mechanical properties of welded joints. The tensile property test was an important index to reflect the mechanical properties of materials. It mainly tested the tensile strength and elongation of materials, and then measures the softening degree of 6061 aluminum alloy welded joints. The experiment

referred to the ISO 4136-2012 destructive tests on welds in the metallic materials-transverse tensile test for sample selection [18]. In order to ensure that there was no large error in the tensile test, each state parameters to take two specimens. The tensile test was carried out using the WDW-100 Electronic Universal Tester (Changchun Kexin, Changchun, China).

Hardness can reflect the strength of materials. The higher the hardness value of metal materials, the higher the plastic deformation resistance and the higher the strength. Before measurement, the surface of the tested sample was polished with 2000 mesh sandpaper [19,20]. 6061-T6 was subjected to solution strengthening and artificial aging treatment in the production process. Therefore, during the welding process, the welded joint was prone to softening, which often appeared in the weld zone, fusion zone, and heat-affected zone [21]. To reflect the overall hardness distribution of welded joints, the hardness test was carried out along the direction perpendicular to the weld. The schematic diagram of the hardness test points is shown in Figure 2.



**Figure 2.** Distribution of hardness test points.

The hardness test was detected by THVS-5 Vickers hardness tester, adopted a load force of 0.2 kg, and the holding time was 15 s. During the test, the diagonal length of rhombic indentation was recorded, and then the hardness value (HV) was calculated by Formula (1):

$$HV = 1.8544 \frac{F}{d_1 d_2} \quad (1)$$

where  $d_1$  and  $d_2$  are diagonal degrees of indentation (mm).

### 2.3. Microstructure Observation

The microstructure of the 6061 aluminum alloy welded joint was observed by Hitachi SU8010 field emission scanning electron microscope (Tokyo, Japan), while the energy spectrometer was used to carry out compositional analysis to determine the chemical element composition and content of the weld matrix and the second phase. The measured surface should contain a complete welded joint perpendicular to the weld. The scanning samples were subjected to rough grinding, fine grinding, polishing, and corroding. The corrosion agent was Keller reagent (2.5%  $\text{HNO}_3$  + 1.5%  $\text{HCl}$  + 1%  $\text{HF}$  + 95%  $\text{H}_2\text{O}$ ).

In order to further determine the phase composition of the microstructure of the welded joint under different process conditions, the phase analysis of the weld was carried out by XRD-7000 X-ray diffractometer (SHIMADZU, Kyoto, Japan), and the scanning angle range was 20–100.

Nordlys Nano EBSD detector was used to analyze the weld grain size and observe the distribution of precipitates. The samples were polished by sandpaper and electropolishing at  $-25\text{ }^\circ\text{C}$  for 1–2 min at 40 V in  $\text{HClO}_4\text{:C}_2\text{H}_5\text{OH} = 1\text{:}9$  (vol.) solution. The EBSD characterization was carried out on GeminiSEM 300 field emission scanning electron microscopy (Zeiss, Jena, Germany) using a scanning step length of 1.5  $\mu\text{m}$ . Channel5 software was used to analyze the EBSD data.

## 3. Results

### 3.1. Influence of Ultrasonic Power on Mechanical Properties

#### 3.1.1. Analysis of Tensile Strength and Elongation

Figure 3 shows the trend of tensile strength and elongation of ER5356 welded joint assisted by ultrasonic. All tensile specimens were broken in the weld zone. Compared with the welded joint without ultrasonic vibration, both tensile strength and elongation are improved. When the ultrasonic output power is 0 W, the tensile strength and elongation of welded joints are the lowest, which is 154.23 Mpa and 4.17%. When the ultrasonic output

power is 800 W, the tensile strength and elongation are the highest, which is 175.02 Mpa and 4.52%. It is speculated that with the increase of ultrasonic output power, the effect of cavitation and acoustic flow maybe more obvious, and the microstructure of the weld maybe finer, so the mechanical properties of the weld are continuously enhanced.

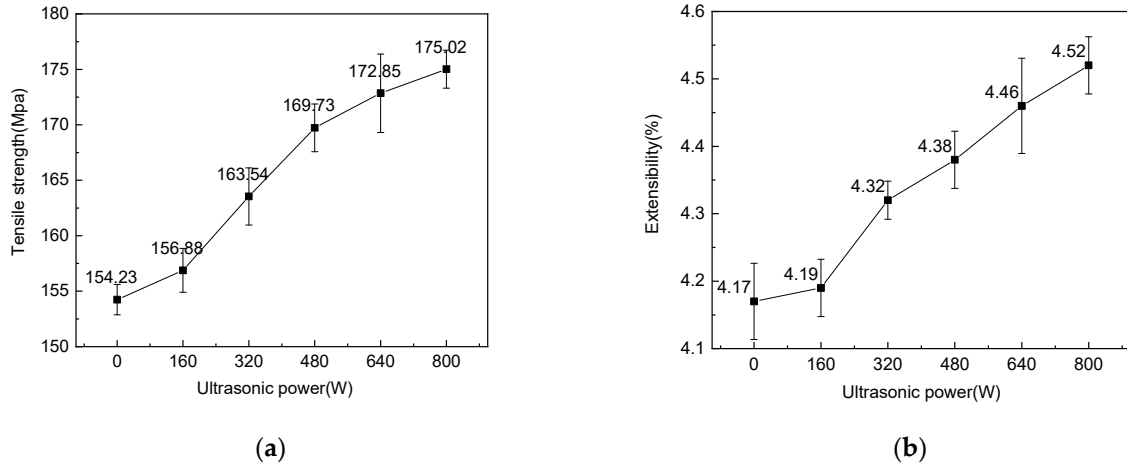


**Figure 3.** Tensile strength and elongation of ER5356 welded joint assisted by ultrasound. (a) Tensile strength. (b) Elongation.

### 3.1.2. Hardness Analysis

Figure 4a shows the trend of the hardness of welded joints with different ultrasonic powers. The hardness of the weld center almost did not change when the ultrasonic output power was 160 W, and it was 78.4 HV. As the increase of ultrasonic output power, the hardness of the weld center had been increasing. and reached the maximum value of 83.5 HV when the ultrasonic output power was 800 W.

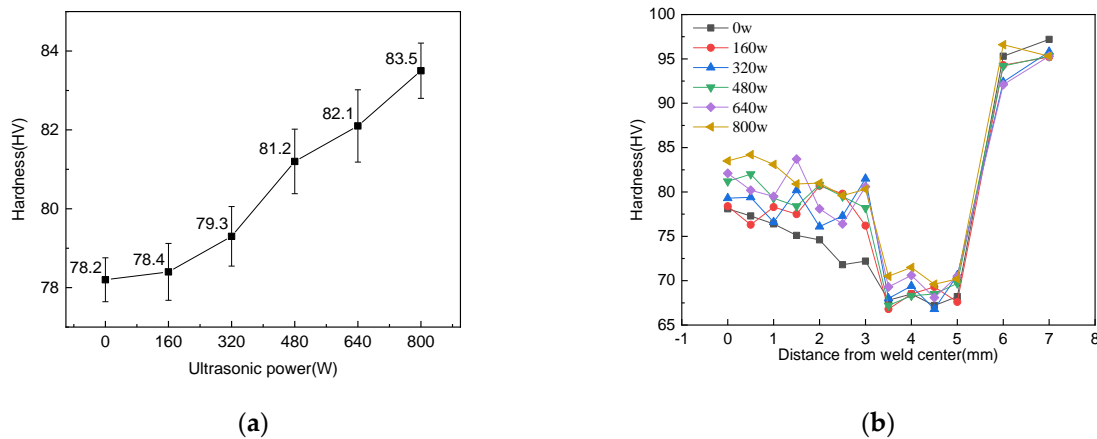


**Figure 4.** Hardness of welded joints with different ultrasonic powers. (a) Change trend of weld center hardness. (b) Hardness distribution of welded joints.

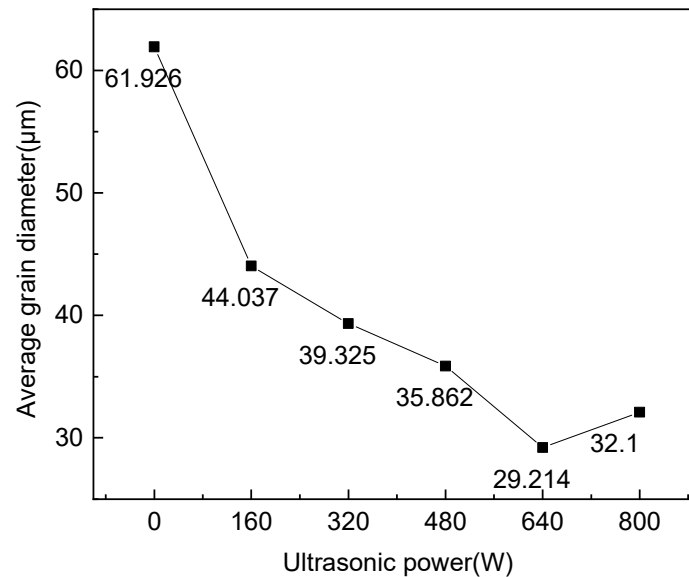
It was speculated that the increase of ultrasonic power made ultrasonic vibration increases continuously, and the effect on welding pool metal became more and more sufficient. In the solidification process of the weld pool metal, the ultrasonic vibration broke the growing grain to form more nucleation cores. At the same time, the ultrasonic vibration also injects energy into the weld pool to promote the formation of nuclei, which in turn played a role in refining the grains, and the hardness of the weld center increases naturally.

Figure 4b shows the hardness distribution of welded joints under different ultrasonic output powers. Compared to the base material area, the hardness of the welded joint is significantly reduced, and the softening of the heat-affected zone location was the most

serious. The location of the heat affected zone was between 3.5 and 6 mm. It was found that the hardness of heat-affected zone increased slightly but did not change much. The average hardness of heat affected zone increased from 66.53 HV to 70.45 HV, only an increase of 2.45 HV. Under the same welding current, the heat input was constant, and the overall heat dissipation capacity of the ultrasonic vibration platform was limited. The heat-affected zone was mainly affected by the heat cycle, and the ultrasonic vibration had no effect on the performance of the heat-affected zone.

### 3.2. Effect of Ultrasonic Power on Grain Size

The average grain size of welded joint under every ultrasonic power was calculated by channel5 software, the results are shown in Figure 5. Before calculation, noise reduction was carried out to decrease the error. With the increase of ultrasonic power, the grain size gradually decreased, until the minimum value is reached 29.214  $\mu\text{m}$  when the ultrasonic power is 640 W. When the ultrasonic power is 800 W, the average grain size does not continue to decrease. Ultrasonic vibration does refine the grain in the weld center, but grain size does not decrease continuously with the increase of ultrasonic power, it has a certain limit.



**Figure 5.** Grain size of weld under different ultrasonic power.

The application of ultrasonic vibration in the cooling and solidification process of the molten pool was conducive to promoting the occurrence heterogeneous nucleation and the nucleation activity of solid particles, thereby increasing the nucleation rate [22–24]. The grains that were growing up were broken, becoming nucleation particles in the center of the molten pool, increasing the number of nucleation particles. Ultrasonic vibration inhibits the growth of grains, so that the microstructure in the weld was fine.

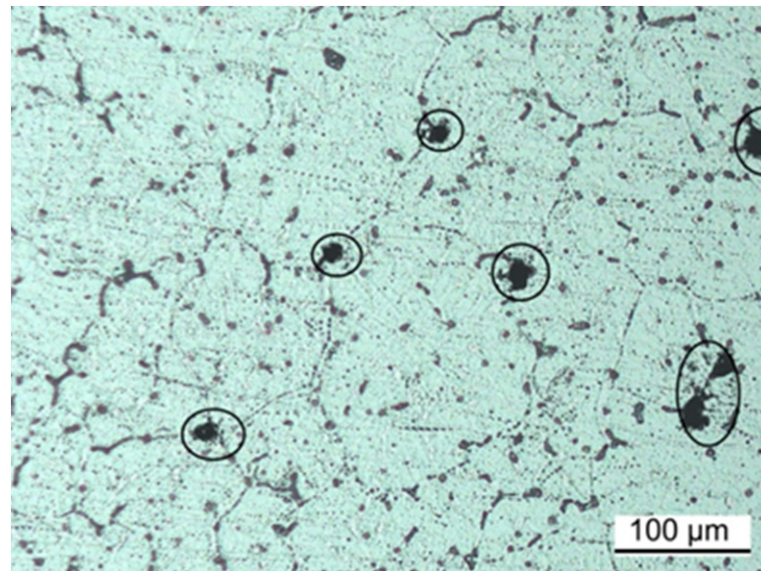
Ultrasound with strong penetrating power may has cavitation effect, with cavitation occurring when the acoustic pressure amplitude exceeds the Blake threshold [25]. The Blake threshold is calculated from Formula (2).

$$P_B = P_0 \left( 1 + \sqrt{\frac{4 S^3}{27 (1 + S)}} \right), \quad S = \frac{2\sigma}{R_0 p_0} \quad (2)$$

where  $p_0$  is the ambient pressure,  $\sigma$  the interfacial tension and  $R_0$  is the initial radius of the bubble, an interfacial tension for aluminium and air of  $\sigma = 1.1 \text{ N/m}$ , and with  $p_0 = 101,325.0 \text{ Pa}$ .



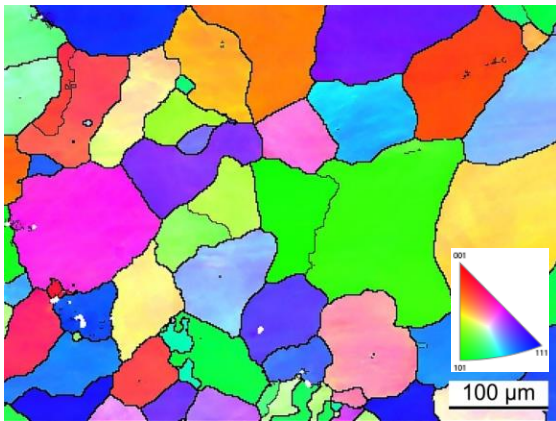
However, the binding force between liquid molecules is very strong. The spontaneous nucleation process of cavitation nuclei generated by ultrasound usually requires large energy, the cavitation threshold is high, and the cavitation effect rarely occurs in theory. In fact, pores are easy to occur during aluminum alloy welding. As shown in Figure 6, there are many small bubbles and impurities in the molten pool, the continuity of the liquid is destroyed, and the bubbles themselves can also be used as cavitation nuclei, resulting in a greatly reduced cavitation threshold in the molten pool. Cavitation can occur under the ultrasonic action of relatively small energy [26,27].



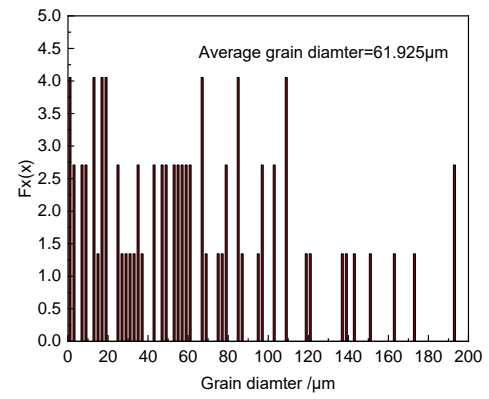
**Figure 6.** Pores in aluminum alloy welded joints.

Figure 7 shows the grain structure by EBSD and the proportion of different grain sizes at different ultrasonic powers. When ultrasonic vibration with power of 320 W was added in the welding process, there are basically no large grains in the weld center with no ultrasonic, and there is rather nucleation of new smaller grain and deformation for others under the ultrasonic vibration. When the ultrasonic power reaches 640 W, the proportion of smaller grains is larger, the weld metal mean grain size could be reduced significantly from  $\sim 61.926 \mu\text{m}$  to a saturated size of  $29.214 \mu\text{m}$ , which is only 47.176% when ultrasonic vibration is not applied. When the ultrasonic power continues to increase to 800 W, the average grain size does not continue to decrease, but the weld center is still small, and the grain accounts for a large proportion.

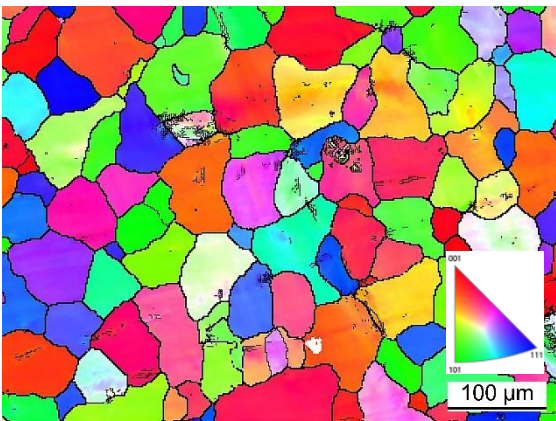
The cavitation bubbles in liquid vibrate under the action of acoustic waves, and the dynamic process of growth and collapse occurs when the acoustic pressure reaches a certain value. The high-speed collapse of these cavitation bubbles will make the surrounding melt generate high temperature and high pressure instantaneously. In this process, the instantaneous temperature and pressure increase the freezing point of the alloy, and accordingly increase the condensate depression of the melt and promote nucleation. In addition, the high temperature generated by cavitation will also make the grains fuse and increase the number of nucleation cores, thus increasing the number of grains. It may also be that strong acoustic waves break up the primary crystal and growing nucleus, thereby inhibiting the growth of grains [28].



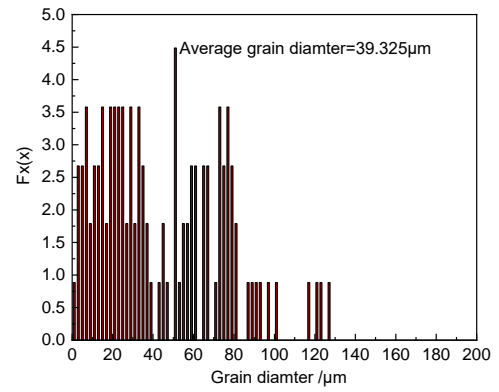
(a)



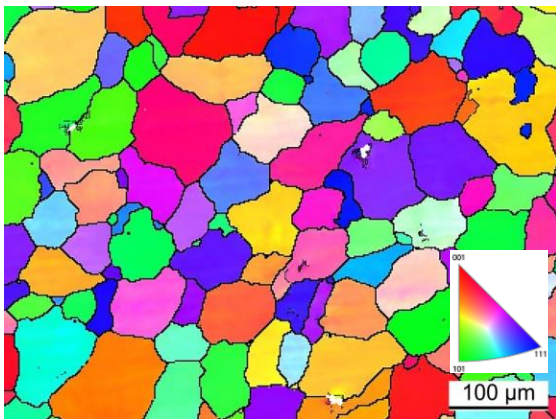
(b)



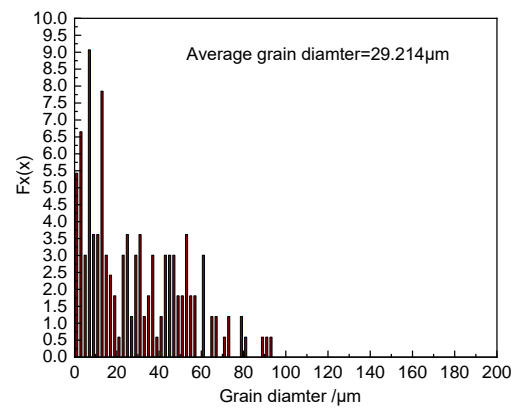
(c)



(d)



(e)



(f)

Figure 7. Cont.



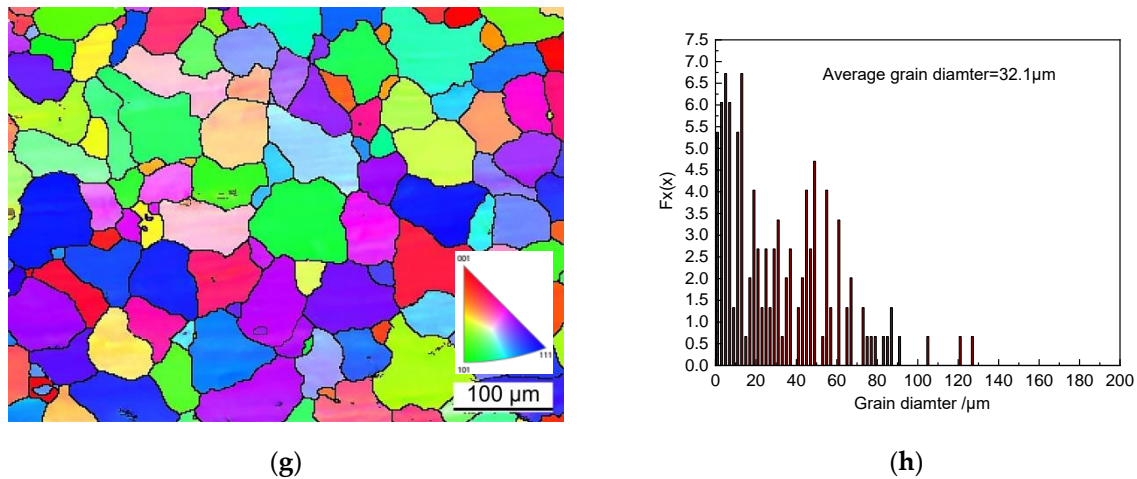


**Figure 7.** The grain structure by EBSD and the proportion of different grain sizes at different ultrasonic powers. (a) Grain structure by EBSD ( $P = 0$  W). (b) Proportion of different grain sizes ( $P = 0$  W). (c) Grain structure by EBSD ( $P = 320$  W). (d) Proportion of different grain sizes ( $P = 320$  W). (e) Grain structure by EBSD ( $P = 640$  W). (f) Proportion of different grain sizes ( $P = 640$  W). (g) Grain structure by EBSD ( $P = 800$  W). (h) Proportion of different grain sizes ( $P = 800$  W).

Second is the acoustic flow effect of ultrasonic waves. The sine wave emitted by ultrasonic causes the aluminum liquid to flow and spray, which prevents the growth of the crystal nucleus and leads to grain refinement. The ultrasonic acoustic flow promotes the heat transfer and diffusion of elements, and accelerates the re-resolution of grains. Due to the turbulent effect caused by the acoustic flow effect of ultrasonic vibration, the flow at the edge of the molten pool is accelerated, and the elements gathered at the grain boundary are stirred to the center of the molten pool. The composition in the molten pool is uniform, which tends to make the temperature gradient in the liquid phase uniform [29,30]. The anisotropy of the crystal is suppressed, which is conducive to the growth of the equiaxed crystal.

According to Formula (3), if the flow is assumed to be frictionless, the liquid phase flow rate caused by acoustic flow can be obtained [31]. When the ultrasonic frequency is 28 kHz and the amplitude is 15  $\mu\text{m}$ , the maximum rate of liquid phase generation can be 1.866 m/s.

$$V = \sqrt{2\pi f A} \quad (3)$$

In which  $V$  is the maximum velocity of liquid phase flow (m/s),  $f$  is the ultrasonic frequency (Hz), and  $A$  is the amplitude ( $\mu\text{m}$ ).

According to Hall–Petch formula (4), ultrasonic vibration acts on the molten pool, under the effect of cavitation and turbulence, the flow rate is accelerated, the nucleation rate is increased, and the growth of crystal nucleus is inhibited. The grain size is reduced [32], the grain boundary is increased, the resistance to slip increases, and the mechanical properties of the weld joint are enhanced.

$$\sigma_y = \sigma_0 + \frac{k_y}{\sqrt{d}} \quad (4)$$

In this formula,  $\sigma_y$  is the yield limit of weld metal (MPa),  $\sigma_0$  is the resistance of a single lattice when moving dislocations (MPa),  $k_y$  is the Hall–Petch coefficient, and  $d$  is the average grain diameter.

Combined with the experimental results of mechanical properties, the fine grain reinforcement improved the tensile strength and hardness of the welded joint, but the grain refinement increased the grain boundaries and hinders the slip of the dislocations, resulting in the increase of elongation was not obvious. The grain size hardly continued to decrease after reaching 29.214  $\mu\text{m}$ , but the tensile strength and hardness of the welded joint

continued to increase, indicating that ultrasonic vibration should have other mechanisms to improve mechanical properties.

### 3.3. Influence of Ultrasonic Power on Precipitated Phase

#### 3.3.1. SEM and EDS Analysis

Figure 8 is SEM analysis of ER5356 Al-Mg welded joint weld. Comparing the SEM and EDS of the matrix and precipitates of ER5356 welded joint before and after ultrasonic vibration, it was found that the types of precipitates in the weld do not change, but their distribution is affected by ultrasonic vibration. The specimen with ultrasonic output power of 800 W was selected for analysis. Figure 8a is the SEM image of the weld zone of the welded joint without ultrasonic vibration. After analyzing the image, it can be seen that most of the precipitates in the weld are distributed along the grain boundary. Figure 8b is the SEM image of the weld area of the welded joint after applying 800 W ultrasonic vibration. Compared with Figure 8a, it can be seen that the precipitates in the weld are more evenly distributed. Under the action of ultrasonic vibration, the precipitates are no longer biased at the grain boundary and redistributed.

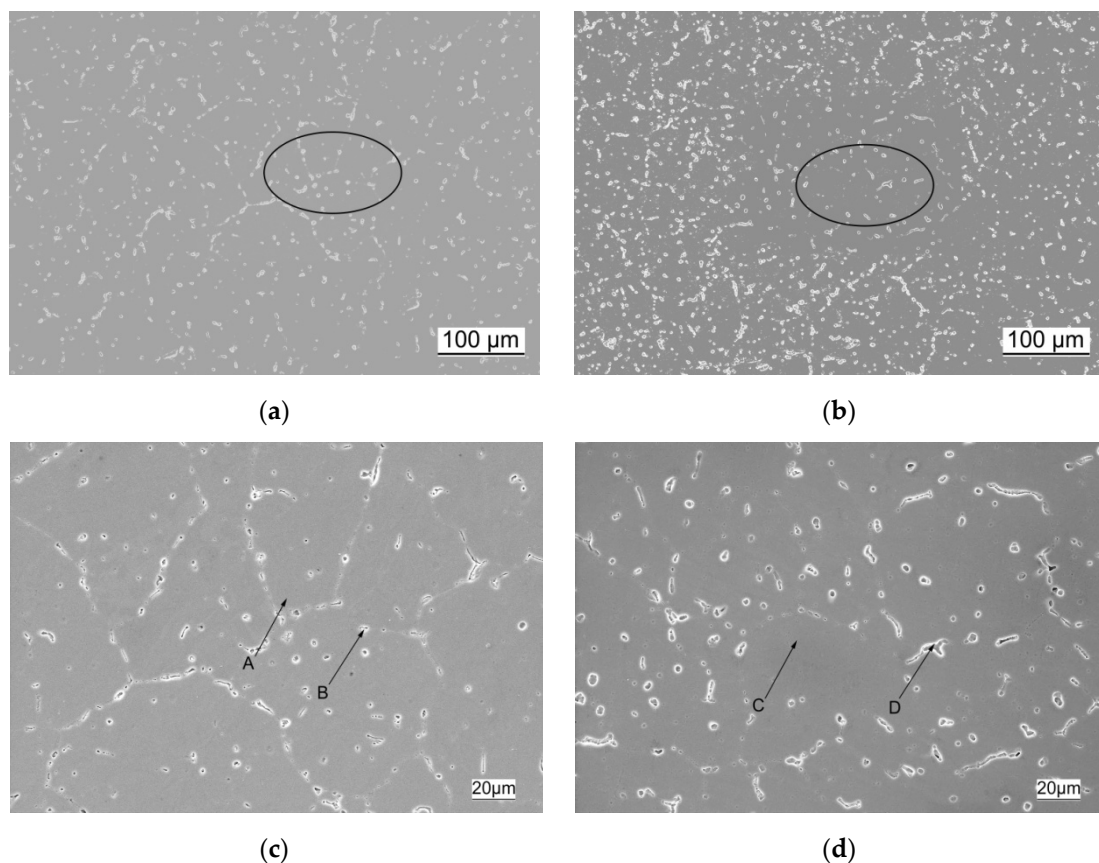


**Figure 8.** ER5356 SEM analysis diagram of the weld seam of aluminum-magnesium welded joint. (a)  $P = 0$  W ( $\times 200$  ML). (b)  $P = 800$  W ( $\times 200$  ML). (c)  $P = 0$  W ( $\times 500$  ML). (d)  $P = 800$  W ( $\times 500$  ML).

In order to make the results of chemical analysis, the morphological organization was enlarged and selected for EDS inspection by high magnification scanning, as shown in Figure 8c,d. After EDS inspection and analysis of the weld structure, it was found that the elements in the weld were nearly identical to those in the base metal, but the main elements were Al, Mg, Si, Cr, and Fe due to the influence of welding filler elements on the weld elements. Si and Fe in the ER5356 welded joint were mainly from the base metal, and Mg was mainly from the ER5356 Al-Mg welding wire. The transition of the Mg element can supplement the burning loss at high current. At the same time, Mg was a strengthening element, forming a strengthening phase, so that the strength of the welded

joint was improved. Table 3 shows the energy spectrum analysis of matrix and precipitated phase of the welded joint. In order to ensure the accuracy of the data, the results in Table 3 are derived from the average value of five points and calculation the errors by Origin software. The analysis results show that the content of Mg and Al was the highest in the weld matrix, and Mg not only formed the precipitation phase, but also dissolved in the matrix, which proved that Mg was dispersed in ER5356 welded joint and played the role of intracrystalline strengthening role.

**Table 3.** Energy spectrum analysis of matrix and precipitated phase of welded joint (atomic fraction,%).

	Al	Error	Mg	Error	Si	Error	Fe	Error	Cr	Error
A	96.43	4.23	3.03	0.11	0.37	0.03	0.00	0.00	0.17	0.04
B	95.24	3.12	3.58	0.16	0.53	0.05	0.32	0.02	0.33	0.06
C	95.99	4.18	3.15	0.11	0.26	0.07	0.26	0.05	0.34	0.05
D	86.83	2.89	5.56	0.39	2.73	0.12	1.46	0.09	3.42	0.13

By comparing the element content of the weld before and after the application of ultrasonic vibration, the change in element contents was due to the transition from the base metal to the weld pool, because the base metal and welding wire were unchanged and no other components were added to the weld. According to the principle of cavitation, at the junction of the molten pool and the base metal, ultrasonic cavitation produces high-temperature point melting and impact, which promoted the dissolution of the base metal side of the fusion zone to the molten pool. At the same time, due to the continuous scouring of the base metal by acoustic flow, it will also lead to the transition of Si, Fe, Cr, and other elements in the base metal to the molten pool. Under the stirring of the two effects, the temperature gradient in the molten pool is uniform, and the elements in the weld are evenly distributed, but it does not affect the types of precipitates in the weld.

### 3.3.2. Phase Analysis

The phase composition of 6061 aluminum alloy weld was measured by X-ray as shown in Figure 9. The elements in the weld area did not change before and after ultrasonic vibration. The types of precipitated phases were completely consistent under each ultrasonic powers. The weld zone mainly contained  $\alpha$ -Al solid solution,  $Mg_2Si$ , and FeCr precipitated phases, which was in line with the speculated results in EDS. The Mg element in ER5356 excessively entered the weld through the droplets, supplemented the burning loss of Mg element caused by high temperature and formed  $Mg_2Si$  strengthening phases with Si element, thus avoiding the formation of cracks in the imbalance between Si and Fe in aluminum alloy. Meanwhile, Cr element can form a small granular Fe-Cr phase with Fe element as reinforcement to avoid the existence of Fe in the weld as needle-like hard and brittle phase, which can reduce the brittleness of the structure.

As an Al-Mg-Si alloy, the aging process of 6061 aluminum alloy is SSSS (supersaturated solid solution) - $\alpha$  (Al)  $\rightarrow$  Cluster  $\rightarrow$  GP zone (solute atom enrichment zone)  $\rightarrow \beta'' \rightarrow \beta'$  (metastable phase)  $\rightarrow \beta$  (equilibrium phase) - $Mg_2Si$  (+Q), and the  $Mg_2Si$  phase is the main strengthening of this alloy [33]. During the Al-Mg-Si alloy limitation process, it grows up rapidly and becomes needle- or rod-like along the [100] direction of the matrix, which is called the  $\beta'$  transition phase. The  $\beta'$  phase keeps a completely coherent relationship with the matrix and produces a co-lattice distortion during the transition to the  $\beta$  equilibrium phase, forming a strong stress field, hindering the motion of the dislocation, and improving the strength and hardness of the alloy. The main composition of 6061 aluminum alloy is  $\alpha$  (Al) +  $Mg_2Si$  two-phase eutectic. However, under the influence of the welding thermal cycle, the increase in temperature makes the  $\beta$  phase transform into the  $\beta'$  transition phase which is locally coherent with the matrix, and the hindrance to dislocation movement decreases. The peak value of hardness and strength of the alloy appears at the end of the  $\beta$  phase and the beginning of the  $\beta'$  phase, and then its strength and hardness begin

to decrease. At last, the  $\beta$  ( $\text{Mg}_2\text{Si}$ ) stable phase is formed at the interface between the  $\beta'$  transition phase and the matrix by consuming  $\beta'$  transition phase. However, the coherent relationship between  $\beta$  ( $\text{Mg}_2\text{Si}$ ) phase and matrix is destroyed, and the coherent distortion also disappears. With the increase of temperature and time, the particles of the  $\beta$  ( $\text{Mg}_2\text{Si}$ ) phase gather and coarsen, the strengthening effect disappears, and the strength and hardness of the alloy further decrease, resulting in averaging softening [34].

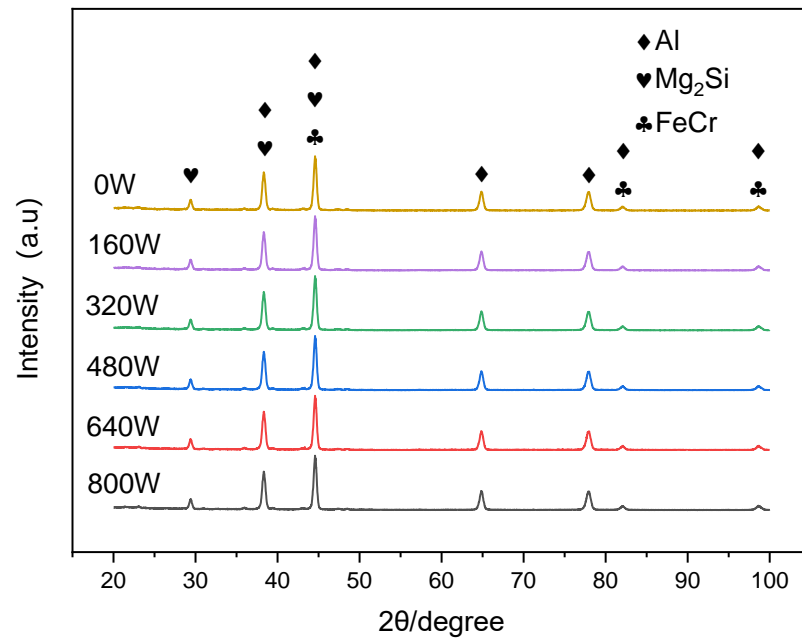


**Figure 9.** XRD spectra of welded joints with different ultrasonic powers.

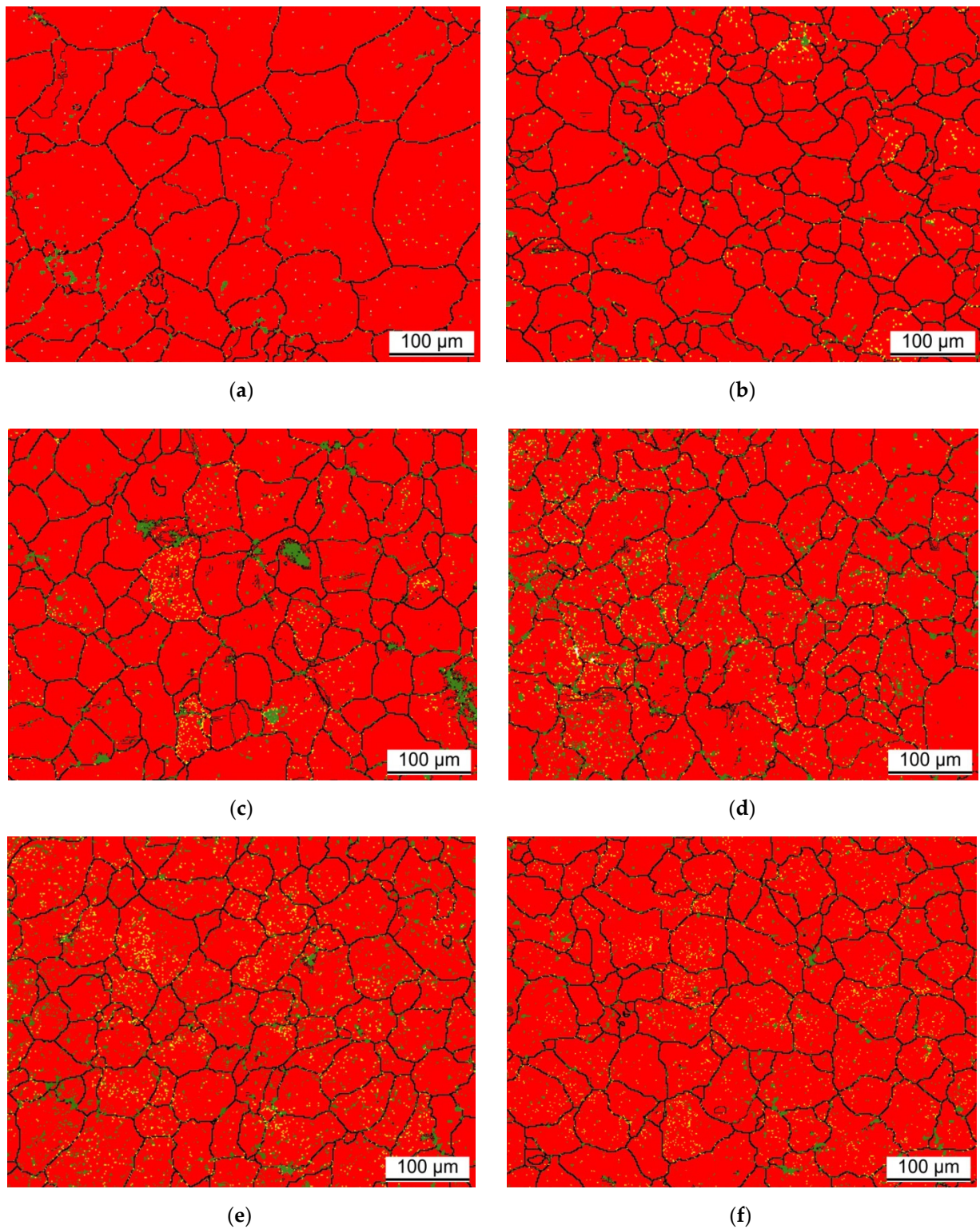
### 3.3.3. Analysis of Phase Distribution

Figure 10 shows the distribution of each precipitated phase in the center of the weld under different ultrasonic power, in which red is  $\alpha$  (Al) matrix, yellow is  $\text{Mg}_2\text{Si}$ , and green is FeCr. Figure 10a shows the distribution of precipitated phases when ultrasonic vibration is not applied, with few precipitated phases and segregation phenomenon. With the increase in ultrasonic power, the precipitated phases gradually increase; the proportion of each phase under different ultrasonic power is shown in Table 4. A large number of precipitated phases had appeared in the weld center at 320 W, compared with no ultrasonic vibration;  $\text{Mg}_2\text{Si}$  increased from 0.18% to 1.23%, and FeCr increased from 1.42% to 4.46%. However, the segregation phenomenon was very obvious,  $\text{Mg}_2\text{Si}$  phase was distributed in individual grains, and the FeCr phase is obviously gathered at grain boundaries. With the increase of ultrasonic power, the number of precipitated phases gradually tends to be flat, and they are uniformly distributed in the crystal and grain boundary as finely dispersed particles.

**Table 4.** Proportion of each phase in the center of welded joint under different ultrasonic power.

	0 W	160 W	320 W	480 W	640 W	800 W
$\text{Mg}_2\text{Si}$	0.18	0.72	1.23	2.33	2.37	2.32
FeCr	1.42	2.38	4.46	4.38	4.65	4.01
Al ( $\alpha$ )	98.40	96.90	94.13	93.29	92.98	93.67





**Figure 10.** Phase distribution diagram of the center of the welding joint under different ultrasonic power. (a)  $P = 0$  W. (b)  $P = 160$  W. (c)  $P = 320$  W. (d)  $P = 480$  W. (e)  $P = 640$  W. (f)  $P = 800$  W.



Ultrasonic vibration propagates in the liquid phase to produce acoustic streaming and form a turbulence effect. When propagating in the liquid phase, there will be energy loss and form a sound pressure gradient. This effect was formed at the solid–liquid interface and propagates from the solid phase to the liquid phase, which can increase the plastic flow of metal and stir the micron-sized medium evenly [35]. In addition, the action of ultrasonic can accelerate the reaction speed of substances, reduce the requirements of environmental conditions required for chemical reactions, initiate reactions that were generally difficult to produce, shorten the reaction induction time, or improve the reaction yield. The influence of ultrasonic vibration on precipitated phase is divided into two stages. The first stage is to increase the number of the precipitated phase. Because ultrasonic vibration improves the fluidity of the molten pool, the alloy elements in the base metal transition to the weld, and the number of precipitated phase increases. The next stage is to change the distribution of precipitates. Because the second phase is easier to form at the grain boundary and aggregate to cause segregation, the stirring effect of ultrasonic vibration on the molten pool makes the second phase evenly distributed, and the precipitates at the grain boundary are gradually evenly distributed into the crystal. Therefore, with the increase of ultrasonic power, the alloying element degree of the base metal passing through the weld increases gradually, and the number of precipitates formed in the weld increases gradually, and the distribution is gradually uniform.

Combined with the experimental results on mechanical properties, dispersion strengthening also had an effect on the strength and hardness of the welded joint. When the grain size did not continue to decrease, dispersion strengthening played a major role in the improvement of mechanical properties. However, the precipitation of the second phase had a pinning effect on the dislocations and hindered the improvement of the plasticity of the welded joint. The change in mechanical properties of the welded joint was the result of the combined effect of fine grain strengthening and dispersion strengthening.

#### 4. Conclusions

In this research, the ultrasonic vibration assisted welding of 6061 aluminum alloy sheet is studied, and the conclusions are as follows:

Applying ultrasonic vibration to TIG welding can improve the mechanical properties of welded joints. When the ultrasonic output power reaches 800 W, the tensile strength of the weld is 173.02 Mpa, and the hardness of the weld center is 83.5 HV, but it has little effect on the heat affected zone.

Ultrasonic-assisted TIG welding can produce cavitation effect and sound flow in the weld pool and refine the weld grain. When the ultrasonic power is 640 W, the grain size decreases by nearly 50%, and the ultrasonic power continues to increase, but the grain size will not continue to decrease. Grain refinement can enhance the strength and hardness of the weld, but grain refinement increases the grain boundaries, hinders the slip of dislocations, and makes the toughness of the weld change less.

In the welding process, the sound flow generated by the external ultrasonic vibration in the molten pool accelerates the flow of the molten pool, makes the base metal transfer more elements to the inside of the weld, increases the number of precipitates in the weld, and makes the precipitates in the weld evenly distributed. As a strengthening phase, the precipitates improve the softening of the weld area.

In summary, adding ultrasonic vibration during fusion welding can improve the mechanical properties of aluminum alloy welded joints, and there is an ultrasonic power to minimize the grain size in the weld center. In future studies, the influence of ultrasonic vibration-assisted welding on the weldability of aluminum alloy can also be analyzed to determine whether ultrasonic vibration can improve the welding defects of aluminum alloy such as thermal cracks and pores.

**Author Contributions:** Conceptualization, C.S. and Z.L.; methodology, X.A.; software, Z.Z.; data curation, Z.L.; writing—original draft preparation, C.S. writing—review and editing, C.S.; funding acquisition, C.L. All authors have read and agreed to the published version of the manuscript.

**Funding:** “Basic Scientific Research Project of Higher Education Institutions of Liaoning Province” (No. LZGD2017037).

**Institutional Review Board Statement:** Not applicable.

**Data Availability Statement:** Not applicable.

**Conflicts of Interest:** The authors declare no conflict of interest.

## References

1. Huang, H.Y.; Kuo, I.C.; Zhang, C.W. Friction-stir welding of aluminum alloy with an iron-based metal as reinforcing material. *Sci. Eng. Compos. Mater.* **2018**, *25*, 123–131. [[CrossRef](#)]
2. Dutra, J.C.; Silva, R.H.G.E.; Savi, B.M.; Marques, C.; Alarcon, O.E. Metallurgical characterization of the 5083H116 aluminum alloy welded with the cold metal transfer process and two different wire-electrodes (5183 and 5087). *Weld. World* **2015**, *59*, 797–807. [[CrossRef](#)]
3. Schempp, P.; Cross, C.E.; Schwenk, C.; Rethmeier, M. Influence of Ti and B additions on grain size and weldability of aluminium alloy 6082. *Weld World* **2013**, *56*, 95–104. [[CrossRef](#)]
4. Aldalur, E.; Suárez, A.; Veiga, F. Metal transfer modes for Wire Arc Additive Manufacturing Al-Mg alloys: Influence of heat input in microstructure and porosity. *J. Mater. Process Tech.* **2021**, *297*, 117271. [[CrossRef](#)]
5. Derekar, K.S. A review of wire arc additive manufacturing and advances in wire arc additive manufacturing of aluminium. *Mater. Sci. Tech-Long* **2018**, *34*, 895–916. [[CrossRef](#)]
6. Lei, Z.; Jiang, B.; Peng, L.; Qian, L.; Chen, Y.; Zhang, D. Melt flow and grain refining in ultrasonic vibration assisted laser welding process of az31b magnesium alloy. *Opt. Laser Technol.* **2018**, *108*, 409–417. [[CrossRef](#)]
7. Li, N.; Cui, C.X.; Zhao, Y.Q.; Zhang, Q.X.; Bai, L.N. Structure and properties of GCr15 modified by multiphase ceramic nanoparticles /Fe-C composite inoculants. *Mat. Sci. Eng. A Struct.* **2018**, *738*, 63–74. [[CrossRef](#)]
8. Wang, H.; Zhu, S.; Xu, G.; Zhou, W.; Li, L.; Zhang, D.H.; Ren, N.; Xia, K.; Shi, C. Influence of Ultrasonic Vibration on Percussion Drilling Performance for Millisecond Pulsed Nd:YAG Laser. *Optlaser. Technol.* **2018**, *104*, 133–139. [[CrossRef](#)]
9. Wei, R.R.; Lv, X.W.; Yang, M.R.; Xu, J.; You, Z.X. Improving the property of calcium ferrite using a sonochemical method. *Ultrason. Sonochem.* **2018**, *43*, 110–113. [[CrossRef](#)]
10. Nesvijski, E.G. Some aspects of ultrasonic testing of composites. *Compos. Struct.* **2000**, *48*, 151–155. [[CrossRef](#)]
11. Takuya, Y.; Kazuki, K.; Sergey, V.K. Characterization of acoustic streaming in water and aluminum melt during ultrasonic irradiation. *Ultrason. Sonochem.* **2021**, *71*, 105381.
12. Feng, W.; Dmitry, E.; Jiawei, M.; Chuangnan, W.; Billy, K.; Andrew, K.; Christina, R.; Thomas, C. A synchrotron X-radiography study of the fragmentation and refinement of primary intermetallic particles in an Al-35 Cu alloy induced by ultrasonic melt processing. *Acta Mater.* **2017**, *141*, 142–153.
13. Yuan, J.; Xiao, J.; Li, F.C.; Wang, B.J.; Yao, Z.; Yu, B.L.; Zhang, L.Y. Co-treatment of spent cathode carbon in caustic and acid leaching process under ultrasonic assisted for preparation of SiC. *Ultrason. Sonochem.* **2018**, *41*, 608–618. [[CrossRef](#)] [[PubMed](#)]
14. Xia, H.S.; Wang, Q.; Liao, Y.Q.; Xu, X.; Baxter, S.M.; Slone, R.V.; Wu, S.G.; Swift, G.; Westmoreland, D.G. Polymerization rate and mechanism of ultrasonically initiated emulsion polymerization of n-butyl acrylate. *Ultrason. Sonochem.* **2002**, *9*, 151–158. [[CrossRef](#)]
15. Priyadarshi, A.; Khavari, M.; Subroto, T.; Conte, M.; Prentice, P.; Pericleous, K.; Eskin, D.; Durodola, J.; Tzanakis, I. On the governing fragmentation mechanism of primary intermetallics by induced cavitation. *Ultrason. Sonochem.* **2021**, *70*, 105260. [[CrossRef](#)]
16. Bing, W.; Dongyue, T.; Tung, L.L.; Jia, C.K.; Feng, W.; Dmitry, E.; Thomas, C.; Kamel, F.; Jiawei, M. Ultrafast synchrotron X-ray imaging studies of microstructure fragmentation in solidification under ultrasound. *Acta Mater.* **2018**, *144*, 505–515.
17. Bai, G.Z.; Liu, Z.; Lin, J.X.; Yu, Z.F.; Hu, Y.M.; Wen, C. Effects of the addition of lanthanum and ultrasonic stirring on the microstructure and mechanical properties of the in situ Mg<sub>2</sub>Si/Al composites. *Mater. Des.* **2016**, *90*, 424–432. [[CrossRef](#)]
18. Karabulut, H.; Turkmen, M.; Erden, M.A.; Gunduz, S. Effect of Different Current Values on Microstructure and Mechanical Properties of Microalloyed Steels Joined by the Submerged Arc Welding Method. *Metals* **2016**, *6*, 281. [[CrossRef](#)]
19. Chen, X.D.; Tian, H.C.; Yan, Z.H.; Zhi, X.L.; Zhang, J.; Yuan, Z.J. Investigation on mechanism of surface tension on morphology of melt track in selective laser melting processing. *Appl. Phys. A Mater.* **2018**, *124*, 673. [[CrossRef](#)]
20. Lachowicz, M.M.; Haimann, K.; Lachowicz, M.B.; Jasionowski, R.; Pawlak, S. Structural aspects of corrosion resistance in alloys based on the Fe<sub>3</sub>Al intermetallic phase in the cast state. *Mater. Sci. Poland* **2012**, *30*, 217–225. [[CrossRef](#)]
21. Chowdhury, S.H.; Chen, D.L.; Bhole, S.D.; Powidajko, E.; Weckman, D.C.; Zhou, Y. Fiber Laser Welded AZ31 Magnesium Alloy: The Effect of Welding Speed on Microstructure and Mechanical Properties. *Metall. Mater. Trans. A* **2012**, *43*, 2133–2147. [[CrossRef](#)]
22. Atamanenko, T.V.; Eskin, D.G.; Zhang, L.; Katgerman, L. Criteria of grain refinement induced by ultrasonic melt treatment of aluminum alloys containing Zr and Ti. *Metall. Mater. Trans. A* **2010**, *41*, 2056–2066. [[CrossRef](#)]
23. Easton, M.A.; Stjohn, D.H. A model of grain refinement incorporating alloy constitution and potency of heterogeneous nucleant particles. *Acta Mater.* **2001**, *49*, 1867–1878. [[CrossRef](#)]

24. Nie, K.B.; Wang, X.J.; Hu, X.S.; Xu, L.; Wu, K.; Zheng, M.Y. Microstructure and mechanical properties of SiC nanoparticles reinforced magnesium matrix composites fabricated by ultrasonic vibration. *Mat. Sci. Eng. A Struct.* **2011**, *528*, 5278–5282. [[CrossRef](#)]
25. Tonry, C.E.H.; Djambazov, G.; Dybalska, A.; Griffiths, W.D.; Beckwith, C.; Bojarevics, V.; Pericleous, K.A. Acoustic resonance for contactless ultrasonic cavitation in alloy melts. *Ultrason. Sonochem.* **2020**, *63*, 104959. [[CrossRef](#)]
26. Yao, L.; Hao, H.; Ji, S.H.; Fang, C.F.; Zhang, X.G. Effects of ultrasonic vibration on solidification structure and properties of Mg-8Li-3Al alloy. *T Nonferr. Metal. SOC* **2011**, *21*, 1241–1246. [[CrossRef](#)]
27. Xu, H.; Pu, C. Removal of Near-wellbore Formation Damage by Ultrasonic Stimulation. *Petrol. Sci. Technol.* **2013**, *31*, 563–571. [[CrossRef](#)]
28. Chen, Q.H.; Ge, H.L.; Yang, C.L.; Lin, S.B.; Fan, C.L. Study on Pores in Ultrasonic-Assisted TIG Weld of Aluminum Alloy. *Metals* **2017**, *7*, 2. [[CrossRef](#)]
29. Yuan, D.; Shao, S.Q.; Guo, C.H.; Jiang, F.C.; Wang, J.D. Grain refining of Ti-6Al-4V alloy fabricated by laser and wire additive manufacturing assisted with ultrasonic vibration. *Ultrason. Sonochem.* **2020**, *73*, 105472. [[CrossRef](#)]
30. Wang, Y.P.; Qi, B.J.; Cong, B.Q.; Yang, M.X.; Liu, F.J. Arc Characteristics in Double-Pulsed VP-GTAW for Aluminum Alloy. *J. Mater. Process. Tech.* **2017**, *249*, 89–95. [[CrossRef](#)]
31. Campbell, J. Effects of vibration during solidification. *Int. Metals Rev.* **1981**, *26*, 71–108.
32. Meng, X.D.; Li, H.B.; Chen, J.Y.; Mei, L.; Wang, K.Q.; Li, X. Mossbauer study of cobalt ferrite nanocrystals substituted with rare-earth Y<sup>3+</sup> ions. *J. Magn. Magn. Mater.* **2009**, *321*, 1155–1158. [[CrossRef](#)]
33. Yassar, R.S.; Field, D.P.; Weiland, H. Transmission electron microscopy and differential scanning calorimetry studies on the precipitation sequence in an Al-Mg-Si alloy: AA6022. *J. Mater. Res.* **2005**, *20*, 2705–2711. [[CrossRef](#)]
34. Marioara, C.D.; Nordmark, H.; Andersen, S.J.; Holmestad, R. Post-β" phases and their influence on microstructure and hardness in 6xxx Al-Mg-Si alloys. *J. Mater. Sci.* **2006**, *41*, 471–478. [[CrossRef](#)]
35. Sritharan, K.; Strobl, C.J.; Schneider, M.F.; Wixforth, A.; Guttenberg, Z. Acoustic mixing at low Reynold's numbers. *Appl. Phys. Lett.* **2006**, *88*, 054102. [[CrossRef](#)]